EVALUATION OF THE "SALAR DE UYUNI/BOLIVIA" AS RADIOMETRIC CALIBRATION TEST SITE FOR SATELLITE SENSORS

Flávio Jorge PONZONI

Instituto Nacional de Pesquisas Espaciais (INPE) - Divisão de Sensoriamento Remoto
Avenida dos Astronautas, 1758 - 12227-010 - São José dos Campos SP - Brasil
flavio@ltid.inpe.br

Rubens LAMPARELLI, Giampaolo Queiroz PELLEGRINO, Jurandir ZULLO JUNIOR

Universidade de Campinas (UNICAMP) - Centro de Ensino e Pesquisa em Agricultura (CEPAGRI)
Cidade Universitária "Zeferino Vaz"- Barão Geraldo - Campinas SP - Brasil
rubens@cpa.unicamp.br, giam@cpa.unicamp.br, jurandir@cpa.unicamp.br

ABSTRACT

The "Salar de Uyuni"(Bolivia) has been pointed out as a potential reference site for spectral calibration purposes (Price, 1987). TM/Landsat 5 images from 1988 to 1997 were used in order to evaluate the spectral characteristics of the "Salar de Uyuni" surface. It was considered images of six TM spectral bands (band 1, 2, 3, 4, 5 and 7) which were used to calculate Variation Coefficients (VC) values for each pixel in each spectral band. These VC values were exchanged by color tones and VC images were created. It was possible to evaluate the spectral stability of the "salar" surface for each TM band through the VC images. The results have pointed out that the "salar" surface is not so stable as could be firstly supposed, mainly in infrared region in which surrounding areas were identified as more stable for this spectral region. Radiometric measurements were performed in field in order to compare them to orbital data.

1 INTRODUCTION

The substantial increasing on the number of operational and to-launch satellites and on the quantitative use of its information requires a parallel increasing of the knowledge about radiometric behavior of the remote sensors along time. They may suffer changes that should be monitored by periodic calibrations. The calibration methods for natural resource satellites can be grouped in two parts: (a) the pre-launch methods based on laboratory measurements and (b) the post-launch methods based on the observation of celestial bodies (like Sun and Moon) or earth surface targets.

The use of terrestrial targets or calibration sites is the one that presents best results along the satellite lifetime. All calibration sites used or proposed until now are located on north hemisphere like: White Sands (USA), La Crau (France), Sahara and Gobi deserts (respectively on Africa and China). A completely different calibration site in localization (i.e., south hemisphere) and surface type has been suggested by many authors (like Price, 1987) as an ideal alternative for satellite sensors calibration: the Uyuni salt lake in Bolivia called as "Salar de Uyuni". It is a flat area of about 200 x 100 km, at 3700 meters of altitude and covered homogeneously by salt. This means the biggest and higher salty open area in the world. According to literature, the "Salar de Uyuni" has very good characteristics for using it for calibration purposes: small atmospheric influence, spectral stability, high reflectivity and proximity to a contrasting target that is the Titicaca Lake. On this context, the objective of this paper is to analyze the radiometric changes on the Lansat-5/TM satellite sensor along time, and to radiometricaly characterize the "Salar de Uyuni" in order to evaluate it as a sensor calibration site in south hemisphere.

2 METHODOLOGY

2.1 Study area localization

The "Salar de Uyuni" is located in the bolivian "altiplanos", at 3700 meters of altitude, and has a surface of about 200 x 100 km covered homogeneously by salt. The Salar is inside a area delimited by the following geographical coordinates: 20°40'S, 68°17'W, 19° 45'S and 66° 45'W, as shown in Figure 1.

The Salar de Uyuni is the largest salt flat in the world with an area of 9000 square kilometers. Located on the central Andean Altiplano of Bolivia, it is at an elevation of over 3600 meters. The Salar is a structurally depressed basin bordered by the Cordillera Occidental to the west and the Cordillera Oriental to the east. The Salar is partially filled with alluvial and glacial deposits and is underlain by Tertiary and Quaternary rhyolitic ashflow tuffs. The surface of the Salar is an evaporate crust of predominantly porous halite and up to 10m thick. Due to the repeated wet and dry cycles, the surface of the Salar is exceptionally smooth with relief measured in centimeters. Situated in a semiarid climate, the Salar

has an average annual rainfall of about 300 mm. The only water inflow to the Salar is from the Rio Grande de Lipez and from small drainages to the east. During the rainy season, from December to March, the Salar maybe covered with brine to depths of 25 cm; however during the dry season, the brine evaporates to a position at or below the surface.
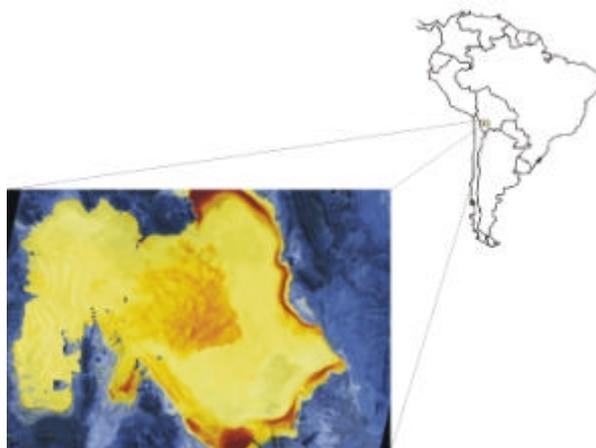

Figure 1 Study area localization

During the Late Pleistocene, the Salar and surrounding areas were drowned under a large lake called Lago Minchin. After the last ice age, the lake began to dry up and large quantities of calcium carbonate were deposited to form marginal algal limestones or high lake stand marks. As the calcium carbonate was removed from the lake, the remaining water became progressively enriched with more soluble saline components like chloride and sulfate. The resulting evaporates with gypsum and finally halite to form the predominantly halite crust. Today the Salar is home to a vast salt mining industry.

The salar surface is covered by a thin water layer during the wet season (from August to March) that changes its apparence towards a typical lake surface. This water layer disappears in the dry season (from April to July) and the salt remains homogeneously distributed in the surface. Table 1 contains the average values of meteorological factors for Salar from 1943 to 1990.

Table 1 – Average values of meteorological factors for Salar from 1943 to 1990.

Data	Jan	Feb	Mar	Apr	May	Jun	Jul	Aug	Sep	Oct	Nov	Dec	Year
Rainfall (mm)	55.3	34.0	23.5	2.3	0.8	2.0	0.0	1.7	3.4	2.0	7.7	32.0	162.4
T_{MIN} (°C)	4.3	4.0	2.8	-2.2	-7.8	-10.2	-11.7	-8.6	-5.8	-2.8	-0.5	2.7	-2.7
T_{MAX} (°C)	20.8	20.3	20.3	18.3	14.6	12.3	12.1	14.4	16.0	18.9	20.8	21.4	17.4
T_{MEAN} (°C)	13.5	12.9	12.8	9.8	5.5	1.9	1.8	4.7	6.4	9.5	11.7	13.4	8.7

2.2 Identification of radiometricaly stable areas

As the drying process does not happen homogeneously and simultaneously in the whole salar surface, spectral differences of reflectance values are expected in all spectral regions. The first step was the identification of stable areas in the salar surface in each TM spectral bands whose reflectance values could be obtained in the field. Reflectance images were obtained transforming ten original radiance images without radiometric or geometric correction (orbit 233, point 74) from 1988 to 1997: 07.12.88, 05.12.89, 03.28.90, 04.16.91, 06.05.92, 04.05.93, 03.23.94, 05.13.95, 04.13.96 and 06.19.97. The first image (07.12.88) was georreferenced using topographic charts on 1:250.000 scale (Villa Martin - SF-19-3; Salinas de Garci Mendoza - SE-19-15; Uyuni - SF-19-4 and Rio Mulato - SE-19-16) and the geographic information system SPRING. The other images were georreferenced using this first image as reference.
The next step was the removal of the atmospheric effects in all images using the SCORADIS system (Zullo Jr., 1994) based on the 5S Model (Tanré, 1986). These corrected images were then used to calculate the Variation Coefficients Images (VC) where each pixel had the variation coefficient of the reflectances values through the ten images. The VC values were sliced using the criteria presented in Table 2.

Different colors were used to distinguish the classes in the VC images. The three more stable areas, considering the spectral behaviour in the visible and near infrared regions, were then chosen as potential ground points to be used in the field measurements. Another point was selected near Hirira town, in the salar's boundary, according to this stability in the near infrared region.
Table 2 - VC classes.

Class	Range (%)	Color and level
1	00-05	Lower (1)
2	06-10	Very Low (2)
3	11-15	Low (3)
4	16-20	Middle Low (4)
5	21-30	Middle (5)
6	31-40	Middle High (6)
7	41-50	Low High (7)
8	51-60	High (8)
9	61-70	High Superior (9)
10	71-80	Very High (10)
11	81-100	Higher (11)

2.3 Field work

The equipments available to perform the radiometric measurements were the following:

- Two radiometers CE313-2/CIMEL, having 6 spectral bands: B1 – 746 to 928nm; B2 – 595 to 701nm; B3 – 464 to 634nm; B4 – 410 to 490nm; B5 – 1475 to 1805nm e B6 - 746 to 928nm;
- A manual sunphotometer CE317/CIMEL, having 5 spectral bands: B1 – 1010 a 1030nm, B2 – 860 a 880nm, B3 – 660 a 680nm, B4 – 430 a 450nm e B5 – 926 a 946nm;
- A thermal infrared radiometer 112.2L/Everest, running from -30° C to $+100^o$ C;
- A spectroradiometer LI1800/LICOR, running from 300 nm to 1100 nm;

The field work was carried out on 1999, June 8th and 9th. The four selected points were visited in the first day when some measurements were done to simulate what would be done during the next day (June 9th) when the Landsat 5 would pass exactly over the region to acquire a new image of the "Salar de Uyuni".

The radiometers CE313-2/CIMEL were used to obtain values of Bidirectional Reflectance Factor (BRF) through consecutive measurements of target and reference radiance (using a $BaSO_4$ standard surface) close to each test point by two people describing a cross trajectory. These measurements were performed from 8:10am to 10:00am on both days, giving more attention to points 1, 2 and 3 in order to measure them close to the satellite pass time on June 9[h]. The radiometer CE313-2/CIMEL was installed 1.75m of height over the surface, defining a sample area of $0.073m^2$.

The LI1800/LICOR was used to collect radiometric data from the point 3 in order to estimate its isotropic properties. The measurements were performed from 12:00am to 17:00pm, each 30 minutes on both days. The target measurements were followed by a reference one using the $BaSO_4$ standard surface in order to determine the BRF.

The sunphotometer was used to measure the direct (sun) and diffuse (sky) radiations in order to get data to characterize the atmosphere. The thermal infrared was used to determine the surface temperatures at the same time the radiometric measurements were performed. Salt samples from the salar surface were also collected to estimate the moisture contents in laboratory.

2.4 Field data processing

The radiance data from the $BaSO_4$ reference surface were also calibrated using a SPECTRALON reference surface. The Bidirectional Reflectance Factors (BRF) were then calculated through the following equation using ground data collected by CE313-2/CIMEL and LI1800/LICOR equipments:

$$R = \frac{ER_s}{EI} = \frac{Cont_s * F}{Cont_p * \in * F} = \frac{Cont_s}{Cont_p * \in}$$

where   R is the surface reflectance factor (BRF);
           ER_s is the reflected energy from the Salar surface;
           EI is the reflected energy by the $BaSO_4$ reference surface;
           $Cont_s$ is the radiometer value presented during the Salar surface measurement;
           $Cont_p$ is the radiometer value presented during the $BaSO_4$ reference surface measurement;

F is an energy unit conversion factor; and

ε is the reflection efficiency of the $BaSO_4$ reference surface.

Mean values of BRF were then calculated using data from several ground points collected during field measurements. Three BRFs averages were calculated for the points inside the salar´s region and two others for the fourth point in the salar's boundary region. These two values were obtained due to the heterogenety of the transition region and because the two teams had described different ways during the measurements.

2.5 Atmospheric characterization

The atmospheric characterization was based on measurements of direct solar radiation using the manual sunphotometer CE317/CIMEL whose output **V** can be given as:

$$V = V_0 . D_S . t_g . \exp(-t.m) \tag{2}$$

where V_0: calibration coefficient;

D_S: Sun-Earth distance factor $(= 1 / \{1 - 0.01673.\cos[0.9856.(J - 4)]\}$, where **J** is the Julian day);

t_g : gaesous transmitance ($\cong 1$ in the spectral regions corresponding to the cimel bands).

t : total optical depth $(= t_{RAYLEIGH} + t_{AEROSOLS}$, where $t_{AEROSOLS}$ is the optical depth to aerosol scattering and $t_{RAYLEIGH}$ is the optical depth due to Rayleigh scattering given by $t_{RAYLEIGH} = (84.35.l^{-4}-1.255.l^{-5} + 1.4.l^{-6}).10^{-4}$. P / 1013.25);

m : air mass number $(= \{1 / [\cos q_S + 0.15.(93.885 - q_S)^{-1.253}]\}.(P/1013.25)$, where **P** is the atmospheric pressure in hPa and q_S is the solar zenith angle).

Applying the natural logarithm in the both sides of this equation, it can be rewritten as:

$$\ln[V / (D_S . t_g)] = \ln V_0 - t.m \tag{3}$$

The plot of $\ln[V / (D_S . t_g)]$ versus **m**, for several solar zenith angles and an assumed stable atmosphere, give the calibration coefficient V_0 (= exp (intercept)) and the total optical depth t (= - slope). This corresponds to the Langley Method.

The measurements of direct solar radiation were performed on June 8th and 9th according to the schedule presented in Table 3. The mean atmospheric pressure **P** during these two days was about 638hPa.

Table 3 – Measurement schedule

Date	D_S	N	First Measurement			Last Measurement		
			Time	q_S	M	Time	q_S	M
June 8th	0.9709	10	9:25h	62.0545	1.3380	16:56h	77.9082	2.9404
June 9th	0.9707	16	8:35h	71.5134	1.9668	16:45h	75.5456	2.4836

The calibration coefficient V_0 and the total optical depth t for each band calculated by the Langley Method are shown in Table 4.

Table 4 – Calibration Results

Cimel Band	$l_{CENTRAL}$ (nm)	R	V_0	t	$t_{RAYLEIGH}$	$t_{AEROSOLS}$
1	1020	0.8902	6792.6743	0.0380	0.0049	0.0331
2	870	0.8089	13542.3060	0.0323	0.0093	0.0230
3	670	0.9771	17970.7372	0.0772	0.0267	0.0505
4	440	0.9963	4296.2593	0.2693	0.1491	0.1202

According to these values, the spectral variation of total optical depth t and aerosol optical depth $t_{AEROSOLS}$ can be given by:

$$t(l) = 0.00623.\exp[1651.527 / l], R = 0,9820, \text{ and} \tag{4}$$
$$t_{AEROSOLS}(l) = 0.008252.\exp[1171.223 / l], R = 0,9440. \tag{5}$$

The last Cimel band (centered on 936nm) was used to estimate the water vapor contents **UW**, considering that the gaseous transmitance by the water vapor t_g is given by the following expression (Zullo Jr., 1996):

$$t_g = \exp [\ -0.6767 \cdot UW^{0.5093} \cdot m^{0.5175}\ ] \qquad (6)$$

Using this expression, the equation used by the Langley Method can be rewritten as

$$\ln [(V \cdot e^{-t \cdot m}) / D_S] = \ln V_0\ - UW^{0.5093} \cdot (0.6767 \cdot m^{0.5175}) \qquad (7)$$

Using the data acquired on June 8th and 9th and considering that $t(0.936\text{nm}) = 0.0364$, the results are: $V_0 = 14341{,}32$, $UW = 0{,}1903\text{g/cm}^2$, $R = 0{,}8208$ for 26 points.

3 RESULTS AND DISCUSSION
3.1 Stable areas and radiometric data collection

Figure 2 shows the VC images for the 6 spectral bands calculated with images from 1988 to 1997.

VC image for band 1

VC image for band 2

VC image for band 3

VC image for band 4

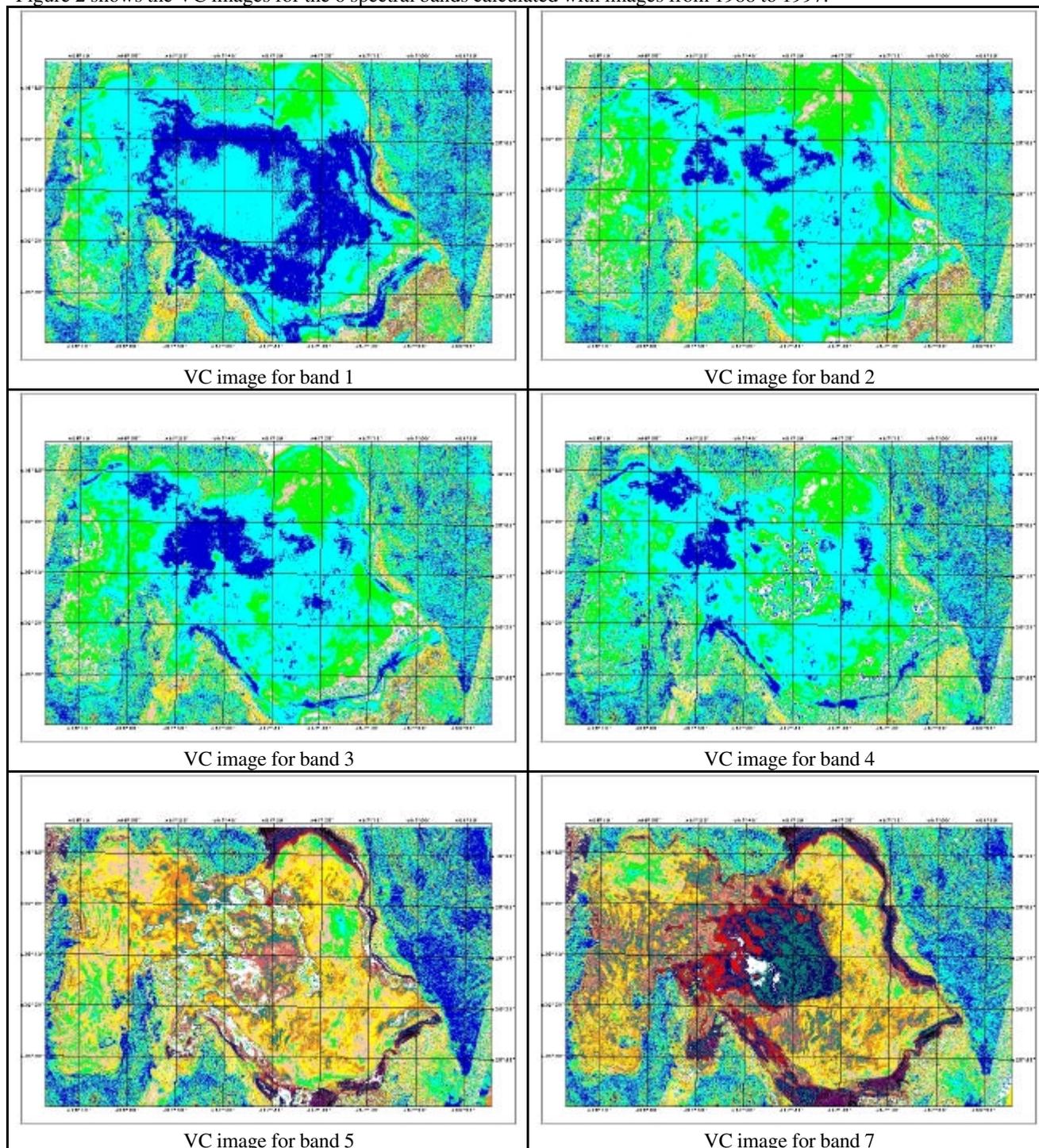VC image for band 5

VC image for band 7

Figure 2 - VC images calculated from 1988 to 1997.

The dark blue areas correspond to the most stable regions while the reddish tones represent the opposite. According to this figure is possible to notice that the "Salar de Uyuni" is not completely radiometric stable as could be firstly supposed but have some stable regions than can be used for calibration purposes. The visible and near infrared bands (bands 1, 2, 3 and 4) have more stable areas in the northwest region. The middle infrared (bands 5 and 7) does not have good stable regions inside the salt surface but some more stable areas outside the Salar that are covered by bare soil and small stones. This behavior (more stable outside than inside the salt surface) can be explained by the great sensibility of the infrared region to the surface water contents since while the inside area is covered by a thin water layer during the wet season, the outside region is still dry. Four points were then selected as potential points to be used in the field mesurements, being three inside the Salar region and another in the transition region. Table 5 shows the four points coordinates.

Table 5 - Four points coordinates.

Point	South Latitude	West Longitude	Point	South Latitude	West Longitude
1	20°00'	64°40'	3	20°05'	67°40'
2	20°00'	67°45'	4	19°52'	67°38'

The values of BRF for each spectral band measured in point 3 are shown in Table 6 and Figure 3.

Table 6- BRF values (%) for each spectral band and local time, measured in point 3 on 1999, June 8th and 9th.

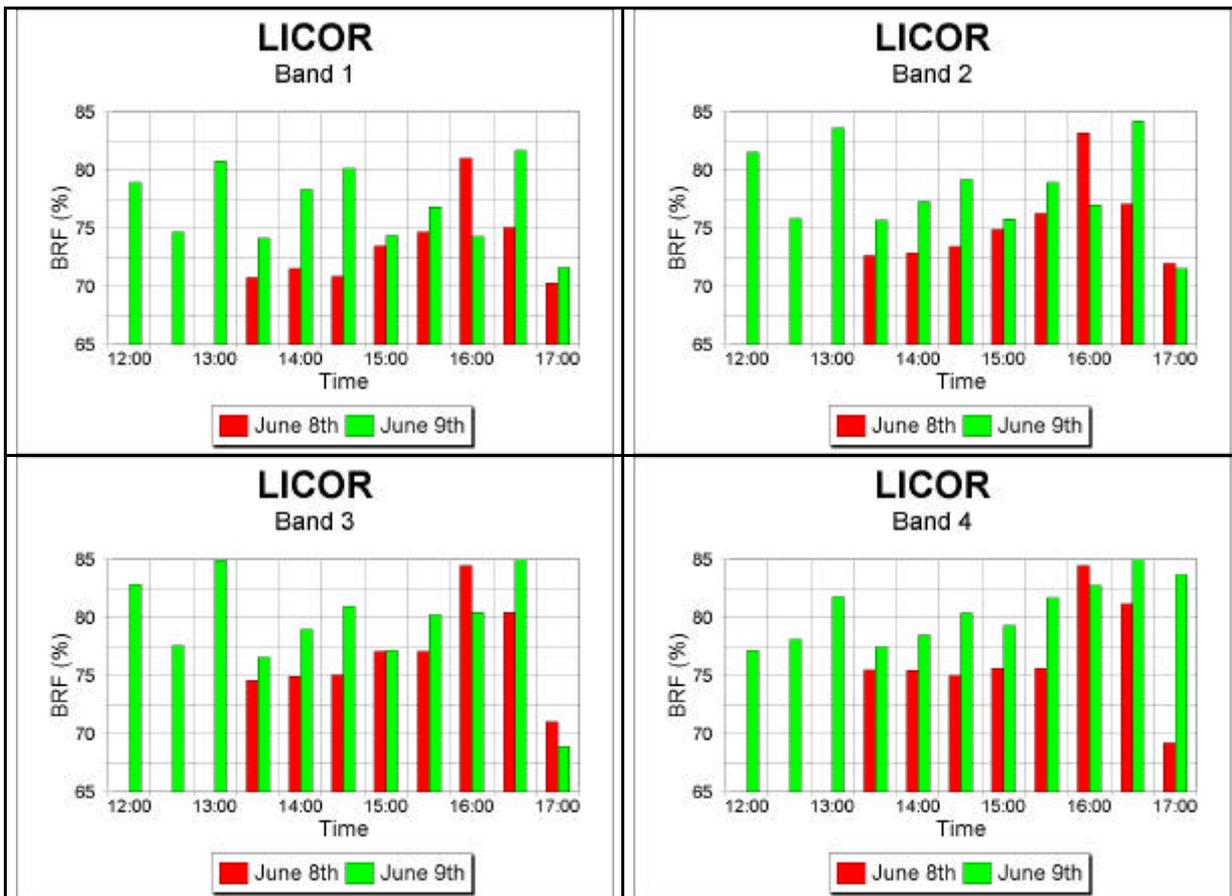| Band	8th (N = 8)			9th (N = 11)			8th and 9th (N = 19)		
	Mean	SD	CV (%)	Mean	SD	CV (%)	Mean	SD	CV (%)
TM1	73.49	3.577	4.77	76.91	3.292	4.28	75.47	3.742	4.96
TM2	75.37	3.667	4.87	78.26	3.790	4.84	77.02	3.927	5.10
TM3	76.86	4.088	5.32	79.56	4.678	5.88	78.42	4.532	5.78
TM4	76.54	4.550	5.94	81.10	3.932	4.85	79.18	4.690	5.92

Figure 3 - BRF values from point 3 using LI1800/LICOR.

Considering the BRFs values on Y axe, it is possible to notice that the BRF variations were relatively small and it was decided to consider that the salar surface has an isotropic behavior. That result was important to understand possible variations in the radiometric measurements that were performed during the satellite pass time, once it was not possible to make all the measurements exactly at the same time. In june 9th, the measurements started as described above:

- **Point 4 (Hirira town):** two teams (using two CIMEL radiometers) collected radiometric data in an area of about 1000m² in the salar's edge from 8:10 am to 8:30 am. This area was covered by stones, bare soil and bushes. Wind speed, surface temperature, diffuse and direct radiation were also measured;
- **Point 1 (stable area):** one of the two teams started the measurements from 9:00 am to 10:00 am. Some measurements were done exately during the satellite pass time;
- **Point 2 (stable area):** another team performed measurements at the same time the first one was collecting data in point 1. In this point 2, there were also collect data from wind speed, surface temperature, diffuse and direct radiation;
- **Point 3 (stable area):** the two teams started to collect data from this point 3 at 12:00 am using the LI-COR 1800.

The BRFs resulting of these measurements are presented on Table 7, which can be compared with some RR values extracted from the atmospheric corrected images.

Table 7 - BRFs values (%) and some RR values (%) extracted from the atmospheric corrected images.

Band 1	Point 1	Point 2	Point 3	Point 4
RR from 1988	56.86	56.86	56.86	12.35
RR from 1999	42.35	42.35	42.35	6.67
BRF (field)	74.86	68.11	68.84	4.25
				1.82
Band 2	Point 1	Point 2	Point 3	Point 4
RR from 1988	77.65	73.73	77.25	10.39
RR from 1999	59.21	59.60	58.82	10.98
BRF (field)	74.73	69.23	67.43	5.46
				6.80
Band 3	Point 1	Point 2	Point 3	Point 4
RR from 1988	78.14	74.51	76.86	13.25
RR from 1999	64.31	64.98	85.88	17.75
BRF (field)	74.71	70.02	66.96	6.37
				6.36
Band 4	Point 1	Point 2	Point 3	Point 4
RR from 1988	76.67	73.45	76.08	15.78
RR from 1999	64.71	65.29	79.22	17.25
BRF (field)	74.58	72.68	66.74	9.75
				13.82
Band 5	Point 1	Point 2	Point 3	Point 4
RR from 1988	44.90	37.25	43.73	18.75
RR from 1999	24.31	30.20	34.51	22.16
BRF (field)	44.52	45.43	38.90	14.12
				16.29
Band 7	Point 1	Point 2	Point 3	Point 4
RR from 1988	19.71	13.92	21.37	11.69
RR from 1999	10.78	13.92	11.18	13.73
BRF (field)	27.41	31.65	23.35	14.84
				6.39

It can be seen that in the visible bands the BRF values were frequentely greater than the respective RR ones, excepting on band 3 where invertions of that happened. For point 4, it noticed that the two BRF averages sometimes were quite different themselves due the heterogeneity of the surface cover (stones, bare soil, bushes etc). Considering the middle infrared bands, it is important to notice that the BRF values were collected from unstable points over the "salar" surface, thus they would not be apropriated to calibration proposes, in spite of having no big differences between both RR and BRF values at band 5 and 7. For these bands, it would be better to consider data collected from point 4 even presenting

heterogeneity on its surface cover. For band 4, "salar's" surface still can be utilized as a reference, but it would be expected less stable points than to visible bands.

4. CONCLUSIONS

Price (1987) belived that the "Salar de Uyuni" could be an interesting reference area in calibration tasks due being a very flat and large surface and having enough radiometric stability. The first characteristic is really true, but the second one had to be evaluate before starting any calibration campaingn. The usage of VC images was a good procedure in order to identify stable areas at the salar surface.

According to the estimated values of aerosol optical depth ($t_{AEROSOLS}$) and water vapor contents ($\mathbf{UW} = 0{,}1903 g/cm^2$), the atmosphere was very clear (horizontal visibility > 30km) and dry during June 8th and 9th that means a very favourable condition of Salar for calibration purposes.

5. KNOWLEDGMENTS

6. REFERENCES

Price, J. C. Radiometric calibration of satellite sensors in the visible and near infrared history and outlook, *Remote Sensing of Environment*, 21:15-27, 1987.

Tanré, D. et al, Description of a computer code to simulate the satellite signal in the solar spectrum: the 5S code. Int.J.Remote Sensing, 1990, vol.11,no.4,659-668.

Zullo Jr.,J. *Correção Atmosférica de Imagens de Satélite e Aplicações*. Tese de Doutorado - Faculdade de Engenharia Elétrica. 1994. 190 p. UNICAMP, Campinas/SP.

Zullo Jr., J., Atmospheric correction of satellite images in a tropical region, *International Archives of Photogrammetry and Remote Sensing*, Vol.XXXI, Part B7, Vienna, 1996, pp.831-834.